Title
Quadratic Response Properties from TDDFT: Trials and Tribulations

Journal
Journal of Chemical Theory and Computation, 14(2)

ISSN
1549-9618

Authors
Parker, Shane M
Rappoport, Dmitrij
Furche, Filipp

Publication Date
2018-02-13

DOI
10.1021/acs.jctc.7b01008

Peer reviewed

Quadratic response properties from TDDFT: trials and tribulations

Shane M. Parker,[†] Dmitrij Rappoport,[†,‡] and Filipp Furche[*,†]

Department of Chemistry, University of California, Irvine, 1102 Natural Sciences II, Irvine, CA 92697-2025, USA

E-mail: filipp.furche@uci.edu

This document is the unedited Authors version of a Submitted Work that was subsequently accepted for publication in *J. Chem. Theory Comput.* ©American Chemical Society after peer review. To access the final edited and published work see dx.doi.org/10.1021/acs.jctc.7b01008.

Abstract

We report on the efficient Turbomole implementation of quadratic response properties within the time-dependent density functional theory (TDDFT) context that includes the static and dynamic dipole hyperpolarizability, ground-to-excited-state two-photon absorption amplitudes (through a single residue) and state-to-state one-photon absorption amplitudes (through a double residue). Our implementation makes full use of arbitrary (including non-Abelian) point-group symmetry as well as permutational symmetry and enables the calculation of nonlinear properties with hybrid density functionals for molecules with hundreds of atoms and thousands of basis functions at a cost that is a fixed multiple of the cost of the corresponding linear properties. Using the PBE0 hybrid density functional, we show that excited-state

[*]To whom correspondence should be addressed

[†]Department of Chemistry, University of California, Irvine, 1102 Natural Sciences II, Irvine, CA 92697-2025, USA

[‡]Department of Chemistry and Chemical Biology, Harvard University, Cambridge, MA 02138, USA

absorption spectra computed within the pseudowavefunction approach contain the qualitative features of transient absorption spectra tracking excimer formation in perylene diimide dimers; two-photon absorption cross sections for a series of highly twisted fused porphyrin chains are semiquantitatively reproduced; and the computed dynamic hyperpolarizability of several calix[4]arene stereoisomers yield simulated hyper-Raleigh scattering signals consistent with experiment. In addition, we show that the incorrect pole structure of adiabatic TDDFT properties can cause incorrect excited state absorption spectra and overly resonant hyperpolarizabilities, and discuss possible remedies.

Nonlinear spectroscopy contains powerful techniques for understanding fundamental light-matter interactions, characterizing complex systems through their high-order properties, and driving novel chemistry.[1] Macroscopic nonlinear behavior of molecular materials is dictated by the nonlinear response function of the molecules that make up the material. For example, the molecular quadratic response function—the first nonlinear response function—encodes the microscopic behavior that leads to processes such as second harmonic generation, sum frequency generation, and the electro-optical Pockels effect.[1]

In addition to the direct description of response properties, response functions are valuable formal tools allowing for the definition of excited state energies and (transition) properties. This approach is especially powerful in the context of approximate electronic structure methods as it provides a definition of excited states and state-to-state properties that requires no explicit wavefunction.[2,3] For example, the poles of the linear response function give excitation energies and their corresponding residues define transition properties between the ground state and an excited state.[2] The quadratic response function contains two-photon absorption amplitudes as single residues[2] and transition properties between two excited states (state-to-state) as double residues.[2]

We present details of a highly resource-efficient implementation of the time-dependent density functional theory (TDDFT) quadratic response function that makes full use of arbitrary point-group symmetry (non-Abelian as well as Abelian), and enables calculations of the static and dynamic hyperpolarizabilities as well as two-photon absorption spectra from the ground state and one-photon

excited-state absorption for molecules with hundreds of atoms and thousands of basis functions.

Several implementations of TDDFT hyperpolarizabilities,[4–15] two-photon absorption spectra,[13,16–20] and excited-state absorption spectra[21–24] have been reported to date and can be found in well established electronic structure codes such as the Dalton program.[25] While pure density functionals (no exact exchange) are known to overestimate (hyper)polarizabilities, the results from hybrid density functionals are greatly improved.[26] However, application of hybrid density functionals to nonlinear optical properties of large molecular clusters and materials has thus far been limited by high computational costs. The implementation detailed here i) is designed to be CPU and memory efficient for use on workstations or single nodes of compute clusters and ii) makes full use of arbitrary (including non-Abelian) point-group symmetry (hyperpolarizability and two-photon absorption) and iii) makes full use of permutational symmetry of the intermediate response densities. As a result, second-order response calculations using hybrid density functionals on molecules with hundreds of atoms and thousands of basis functions are feasible using a single workstation node: the largest calculations reported here involved computing the two-photon absorption amplitudes of 100 excited states for a molecule with 446 atoms and 4548 basis functions.

Recently, we showed that nonlinear response functions defined from any approximate electronic structure methods have an incorrect pole structure that result in unphysical divergences in state-to-state properties.[27] Within TDDFT, the pole structure is cured only by the exact frequency-dependent exchange-correlation (hyper)kernel. Using our new implementation, we expand upon the unphysical behavior of the TDDFT quadratic response function and show specific examples in which a spurious resonance drowns out real features of an excited-state absorption spectrum and the two-photon absorption strength is "over-resonant".

Throughout this paper, the following notation is used: lower-case letters denote single-particle orbitals with $\{i, j, k, l\}$ reserved for orbitals that are strictly occupied in the reference state, $\{a, b, c, d\}$ reserved for orbitals that are strictly unoccupied in the reference state, and $\{p, q, r, s\}$ denoting generic orbitals; upper-case letters denote excited electronic states, $\{N, M, K\}$.

1 Response theory

TDDFT response functions may be derived through several equivalent routes, including density based,[28,29] density matrix based,[30–32] or through the action.[32–34] Second- and higher-order response functions are conveniently derived using the density matrix based approach, in which the response density matrices are defined by enforcing the idempotency and equation of motion of the Kohn–Sham density matrix,

$$\gamma(t, x, x') = \sum_i \varphi_i^*(t, x)\varphi_i(t, x'), \tag{1}$$

order by order where $\varphi_i(t, x)$ is a time-dependent Kohn–Sham orbital. The equation of motion for the Kohn–Sham density matrix is

$$\mathrm{i}\frac{\partial}{\partial t}\gamma = \left[\hat{H}[\rho], \gamma\right], \tag{2}$$

where

$$\hat{H}[\rho] = \hat{T} + \hat{v}(t) + \hat{v}_{\mathrm{HXC}}[\rho], \tag{3}$$

with $\hat{T}$ the kinetic energy operator, $\hat{v}(t)$ the time-dependent external potential, and $\hat{v}_{\mathrm{HXC}}[\rho]$ the Hartree-exchange-correlation potential.[3] The time-dependent field is parametrized as

$$\hat{v}(t) = \sum_\alpha \hat{v}^{(\alpha)}\mathrm{e}^{-\mathrm{i}\omega_\alpha t} + \hat{v}^{(-\alpha)}\mathrm{e}^{\mathrm{i}\omega_\alpha t}, \tag{4}$$

where α labels the perturbation that is oscillating with frequency ω_α, and the requirement that $\hat{v}(t)$ be Hermitian forces $\hat{v}^{(\alpha)} = \left(\hat{v}^{(-\alpha)}\right)^\dagger$.

The first- and second-order idempotency conditions

$$\gamma^{(\alpha)} = \gamma^{(\alpha)}\gamma^{(0)} + \gamma^{(0)}\gamma^{(\alpha)} \tag{5}$$

$$\gamma^{(\alpha\beta)} = \gamma^{(\alpha\beta)}\gamma^{(0)} + \gamma^{(\alpha)}\gamma^{(\beta)} + \gamma^{(\beta)}\gamma^{(\alpha)} + \gamma^{(0)}\gamma^{(\alpha\beta)}, \tag{6}$$

and the first- and second-order equations-of-motion

$$\omega_\alpha \gamma^{(\alpha)} = \left[\hat{H}^{(0)}, \gamma^{(\alpha)}\right] + \left[\hat{H}^{(\alpha)}, \gamma^{(0)}\right] \tag{7}$$

$$\begin{aligned}(\omega_\alpha + \omega_\beta)\gamma^{(\alpha\beta)} = &\left[\hat{H}^{(0)}, \gamma^{(\alpha\beta)}\right] + \left[\hat{H}^{(\alpha)}, \gamma^{(\beta)}\right] \\ &+ \left[\hat{H}^{(\beta)}, \gamma^{(\alpha)}\right] + \left[\hat{H}^{(\alpha\beta)}, \gamma^{(0)}\right],\end{aligned} \tag{8}$$

therefore define the first- and second-order density matrices, where $f^{(\alpha)}$ is shorthand for functional differentiation followed by evaluation at the time-independent field-free Hamiltonian,

$$\left.\frac{\delta f}{\delta v^{(\alpha)}}\right|_{v=v_0} \equiv f^{(\alpha)}. \tag{9}$$

The linear and quadratic response functions are then obtained as expectation values of the first- and second-order density matrices,

$$\langle\!\langle v^{(\beta)}; v^{(\alpha)} \rangle\!\rangle = \mathrm{tr}(\hat{v}^{(\beta)}\gamma^{(\alpha)}), \tag{10}$$

$$\langle\!\langle v^{(\gamma)}; v^{(\alpha)}(\omega_\alpha), v^{(\beta)}(\omega_\beta) \rangle\!\rangle = \mathrm{tr}(\hat{v}^{(\gamma)}\gamma^{(\alpha\beta)}) \tag{11}$$

1.1 Linear response

The TDDFT linear response function can be written as[3]

$$\langle\!\langle v^{(\beta)}; v^{(\alpha)} \rangle\!\rangle = -\langle P^{(\beta)}, Q^{(\beta)} | X^{(\alpha)}, Y^{(\alpha)} \rangle, \tag{12}$$

where the polarization vector $|X^{(\alpha)}, Y^{(\alpha)}\rangle$ parametrizes the off-diagonal blocks of the first-order single-particle reduced density matrix,

$$\gamma^{(\alpha)}(x, x') = \sum_{ia} \left[X_{ia}^{(\alpha)} \varphi_a(x)\varphi_i(x') + Y_{ia}^{(\alpha)} \varphi_i(x)\varphi_a(x')\right], \tag{13}$$

and $|P^{(\zeta)}, Q^{(\zeta)}\rangle$ collects the off-diagonal elements of one-body operator $\hat{v}^{(\zeta)}$, i.e., $P^{(\zeta)}_{ia} = v^{(\zeta)}_{ai}$ and $Q^{(\zeta)}_{ia} = v^{(\zeta)}_{ia}$. The polarization vector is the solution of the linear response equation[3]

$$|X^{(\alpha)}, Y^{(\alpha)}\rangle = -(\Lambda - \omega_\alpha \Delta)^{-1} |P^{(\alpha)}, Q^{(\alpha)}\rangle \tag{14}$$

with linear response super operator

$$\Lambda = \begin{pmatrix} A & B \\ B & A \end{pmatrix} \tag{15}$$

and metric

$$\Delta = \begin{pmatrix} 1 & 0 \\ 0 & -1 \end{pmatrix}. \tag{16}$$

The elements of the linear response super operator—also referred to as the electronic and magnetic orbital rotation Hessians, respectively—are[35]

$$\begin{aligned}(A+B)_{ia,jb} &= (\epsilon_a - \epsilon_i)\delta_{ij}\delta_{ab} + 2f^{\mathrm{xc}}_{ia,jb} + 2(ia|jb) \\ &\quad - c_x[(ib|ja) + (ij|ab)] \qquad (17a)\\ (A-B)_{ia,jb} &= (\epsilon_a - \epsilon_i)\delta_{ij}\delta_{ab} + c_x[(ib|ja) - (ij|ab)], \qquad (17b)\end{aligned}$$

where

$$(pq|rs) = \iint dx\, dx' \varphi_p(x)\varphi_q(x) \frac{1}{|\mathbf{r} - \mathbf{r}'|} \varphi_r(x')\varphi_s(x') \tag{18}$$

is a matrix element of the two-electron Coulomb operator, ϵ_p is the Kohn–Sham orbital eigenvalue for single-particle orbital φ_p, $f^{\mathrm{xc}}_{pq,rs}$ is a matrix element of the exchange-correlation kernel, and c_x is a coefficient that allows one to interpolate between TDHF and TDDFT with pure density functionals. Within the adiabatic approximation to the exchange-correlation functional, the formally

frequency dependent f^{xc} is replaced by its static counterpart, i.e., the second functional derivative of the exchange-correlation energy E_{xc},

$$f^{\mathrm{xc}}(x, x') \approx \left. \frac{\delta^2 E_{\mathrm{xc}}[\rho]}{\delta\rho(x)\delta\rho(x')} \right|_{\rho=\rho_0}, \tag{19}$$

evaluated at the ground state density.

Excited state energies and transition moments are obtained from the poles of the inverse linear response operator,[2] leading to the symplectic eigenvalue equation

$$(\Lambda - \Omega_N \Delta)|X^N, Y^N\rangle = 0, \tag{20}$$

subject to the normalization condition

$$\langle X^N, Y^N|\Delta|X^M, Y^M\rangle = \langle X^N|X^M\rangle - \langle Y^N|Y^M\rangle = \delta_{NM}. \tag{21}$$

Transition moments between the ground state and an excited state[2] are obtained from the excitation vectors as $v_{0N}^{(\alpha)} = \langle v^{(\alpha)}|X^N, Y^N\rangle$.

1.2 Quadratic response

Continuing to second-order, the quadratic response function can be written as[3]

$$\begin{aligned} \langle\langle v^{(\gamma)}; v^{(\alpha)}(\omega_\alpha), v^{(\beta)}(\omega_\beta)\rangle\rangle &= \mathrm{Tr}(\hat{v}^{(\gamma)}\gamma^{(\alpha\beta)}) \\ &= \mathrm{Tr}(\hat{v}^{(\gamma)}K^{(\alpha\beta)}) + \langle P^{(\gamma)}, Q^{(\gamma)}|X^{(\alpha\beta)}, Y^{(\alpha\beta)}\rangle, \end{aligned} \tag{22}$$

where the second-order single-particle reduced density matrix, $\gamma^{(\alpha\beta)}$, is parametrized in terms of the unrelaxed density matrix $K^{(\alpha\beta)}$ (occupied-occupied and virtual-virtual blocks) and the orbital

relaxation contribution $|X^{(\alpha\beta)}, Y^{(\alpha\beta)}\rangle$ (occupied-virtual and virtual-occupied blocks), i.e.,

$$\gamma^{(\alpha\beta)} = \begin{pmatrix} \mathbf{K}^{(\alpha\beta),\mathrm{occ}} & \mathbf{X}^{(\alpha\beta)} \\ \left(\mathbf{Y}^{(\alpha\beta)}\right)^T & \mathbf{K}^{(\alpha\beta),\mathrm{virt}} \end{pmatrix}. \tag{23}$$

$K^{(\alpha\beta)}$ contains simple products of first-order quantities,

$$K_{ij}^{(\alpha\beta)} = -\sum_a \left(X_{ja}^{(\alpha)} Y_{ia}^{(\beta)} + (\alpha \leftrightarrow \beta)\right), \tag{24a}$$

$$K_{ab}^{(\alpha\beta)} = \sum_i \left(X_{ia}^{(\alpha)} Y_{ib}^{(\beta)} + (\alpha \leftrightarrow \beta)\right), \tag{24b}$$

where we have introduced $(\alpha \leftrightarrow \beta)$ to denote the permutation of (α) and (β) in the preceding terms in the parentheses. For the sake of computational efficiency and numerical stability, it is beneficial to separate the totally symmetric and the skew-symmetric contributions to all second-order quantities. To this end, we denote the symmetric and skew-symmetric portions of $K^{(\alpha\beta)}$ by $K^{+(\alpha\beta)}$ and $K^{-(\alpha\beta)}$, respectively, i.e., $K_{pq}^{+(\alpha\beta)} = \frac{1}{2}(K_{pq}^{(\alpha\beta)} + K_{qp}^{(\alpha\beta)})$ and $K_{pq}^{-(\alpha\beta)} = \frac{1}{2}(K_{pq}^{(\alpha\beta)} - K_{qp}^{(\alpha\beta)})$. Furthermore, we replace $X^{(\alpha)}$ and $Y^{(\alpha)}$ by $R^{(\alpha)} = X^{(\alpha)} + Y^{(\alpha)}$ and $L^{(\alpha)} = X^{(\alpha)} - Y^{(\alpha)}$. The unrelaxed second-order density matrix becomes

$$K_{ij}^{+(\alpha\beta)} = -\frac{1}{4}\sum_a \left[R_{ia}^{(\alpha)} R_{ja}^{(\beta)} - L_{ia}^{(\alpha)} L_{ja}^{(\beta)} + (\alpha \leftrightarrow \beta)\right], \tag{25a}$$

$$K_{ij}^{-(\alpha\beta)} = \frac{1}{4}\sum_a \left[L_{ia}^{(\alpha)} R_{ja}^{(\beta)} - R_{ia}^{(\alpha)} L_{ja}^{(\beta)} + (\alpha \leftrightarrow \beta)\right], \tag{25b}$$

$$K_{ab}^{+(\alpha\beta)} = \frac{1}{4}\sum_i \left[R_{ia}^{(\alpha)} R_{ib}^{(\beta)} - L_{ia}^{(\alpha)} L_{ib}^{(\beta)} + (\alpha \leftrightarrow \beta)\right], \tag{25c}$$

$$K_{ab}^{-(\alpha\beta)} = \frac{1}{4}\sum_a \left[L_{ia}^{(\alpha)} R_{ib}^{(\beta)} - R_{ia}^{(\alpha)} L_{ib}^{(\beta)} + (\alpha \leftrightarrow \beta)\right]. \tag{25d}$$

$K^{(\alpha\beta)}$ is neither symmetric nor skew-symmetric with respect to exchange of the orbital indices, but is symmetric with respect to simultaneous exchange of $(v^{(\alpha)}, \omega_\alpha)$ and $(v^{(\beta)}, \omega_\beta)$. This is required by

the symmetry of the quadratic response function,

$$\langle\langle v^{(\gamma)}; v^{(\alpha)}(\omega_\alpha), v^{(\beta)}(\omega_\beta)\rangle\rangle = \langle\langle v^{(\gamma)}; v^{(\beta)}(\omega_\beta), v^{(\alpha)}(\omega_\alpha)\rangle\rangle. \tag{26}$$

The off-diagonal blocks of $\gamma^{(\alpha\beta)}$ require solution of the second-order response equation,

$$|X^{(\alpha\beta)}, Y^{(\alpha\beta)}\rangle = (\Lambda - (\omega_\alpha + \omega_\beta)\Delta)^{-1}|P^{(\alpha\beta)}, Q^{(\alpha\beta)}\rangle, \tag{27}$$

with

$$\begin{aligned}(P+Q)^{(\alpha\beta)}_{ia} = &-\frac{1}{2}\sum_j \left[R^{(\beta)}_{ja}U^{+(\alpha)}_{ji} - L^{(\beta)}_{ja}U^{-(\alpha)}_{ji} + (\alpha \leftrightarrow \beta)\right] \\ &+\frac{1}{2}\sum_b \left[R^{(\beta)}_{ib}U^{+(\alpha)}_{ab} - L^{(\beta)}_{ib}U^{-(\alpha)}_{ab} + (\alpha \leftrightarrow \beta)\right] \\ &+ H^{+}_{ai}[K^{+(\alpha\beta)}] + 2g^{xc}_{ai}[R^{(\alpha)}, R^{(\beta)}], \end{aligned} \tag{28a}$$

$$\begin{aligned}(P-Q)^{(\alpha\beta)}_{ia} = &-\frac{1}{2}\sum_j \left[L^{(\beta)}_{ja}U^{+(\alpha)}_{ji} - R^{(\beta)}_{ja}U^{-(\alpha)}_{ji} + (\alpha \leftrightarrow \beta)\right] \\ &+\frac{1}{2}\sum_b \left[L^{(\beta)}_{ib}U^{+(\alpha)}_{ab} - R^{(\beta)}_{ib}U^{-(\alpha)}_{ab} + (\alpha \leftrightarrow \beta)\right] \\ &- H^{-}_{ia}[K^{-(\alpha\beta)}], \end{aligned} \tag{28b}$$

where we have introduced

$$U^{\pm(\alpha)}_{pq} = H^{\pm}_{pq}[(X \pm Y)^{(\alpha)}] + v^{(\alpha)}_{qp} \pm v^{(\alpha)}_{pq} \tag{29}$$

using the linear transformations

$$H^{+}_{pq}[M] = \sum_{rs} \Big[2(pq|rs) + 2f^{\mathrm{xc}}_{pq,rs} - c_x[(ps|qr) + (pr|qs)] \Big] M_{rs}, \tag{30a}$$

$$H^{-}_{pq}[M] = c_x \sum_{rs} \left[(ps|qr) - (pr|qs) \right] M_{rs}, \tag{30b}$$

and

$$g^{xc}_{pq}[M, M'] = \sum_{rstu} g^{xc}_{pq,rs,tu} M_{rs} M'_{tu}. \tag{31}$$

The previous equations generalize Eq. (39) in Ref. 3 and include a term erroneously omitted in Ref. 3. g^{xc} is the exchange-correlation hyperkernel which reduces to the third functional derivative of the exchange-correlation energy within the adiabatic approximation to the exchange-correlation functional,

$$g^{xc}(x, x', x'') \approx \left. \frac{\delta^3 E_{xc}[\rho]}{\delta\rho(x)\delta\rho(x')\delta\rho(x'')} \right|_{\rho=\rho_0}, \tag{32}$$

evaluated at the ground state density. Again, $(P \pm Q)^{(\alpha)}$ are both symmetric with respect to exchange of $(v^{(\alpha)}, \omega_\alpha)$ and $(v^{(\beta)}, \omega_\beta)$, as required.

Inserting Eq. (27) into Eq. (22) and applying the inverse linear response operator instead to the left yields

$$\begin{aligned} &\langle\!\langle v^{(\gamma)}; v^{(\alpha)}(\omega_\alpha), v^{(\beta)}(\omega_\beta) \rangle\!\rangle = \\ &\quad = \mathrm{Tr}(\hat{v}^{(\gamma)} K^{(\alpha\beta)}) + \langle X^{(\gamma)}, Y^{(\gamma)} | P^{(\alpha\beta)}, Q^{(\alpha\beta)} \rangle \end{aligned} \tag{33}$$

which is a realization of the $2n+1$ rule.

1.2.1 Two-photon absorption amplitudes

From the response theory of exact electronic states one finds that the single residue of the quadratic response function[2,36,37]

$$\lim_{\omega' \to \Omega_N} (\omega' - \Omega_N) \langle\!\langle v^{(\gamma)}(-\omega'); v^{(\alpha)}(\omega), v^{(\beta)}(\omega' - \omega) \rangle\!\rangle = -v_{0N}^{(\alpha\beta)}(\omega) v_{0N}^{(\gamma)} \tag{34}$$

yields the two-photon absorption (2PA) amplitude $v_{0N}^{(\alpha\beta)}(\omega)$. Combining with Eq. (33), the TDDFT 2PA amplitude becomes

$$v_{0N}^{(\alpha\beta)}(\omega) = \langle X^N, Y^N | P^{(\alpha\beta)}, Q^{(\alpha\beta)} \rangle, \tag{35}$$

where $\omega_\alpha = \omega$ and $\omega_\beta = \Omega_N - \omega$ in $P^{(\alpha\beta)}$ and $Q^{(\alpha\beta)}$.

1.2.2 State-to-state transition properties

The double residue of the quadratic response function

$$\lim_{\omega_\alpha, \omega_\beta \to -\Omega_N, \Omega_M} (\omega_\alpha + \Omega_N)(\omega_\beta - \Omega_M) \times \langle\!\langle v^{(\gamma)}; v^{(\alpha)}(\omega_\alpha), v^{(\beta)}(\omega_\beta) \rangle\!\rangle = -v_{0N}^{(\alpha)} \bar{v}_{NM}^{(\gamma)} v_{M0}^{(\beta)}, \tag{36}$$

with $\bar{v}_{NM}^{(\gamma)} = v_{NM}^{(\gamma)} - \delta_{NM} v_{00}^{(\gamma)}$ enables the identification of the state-to-state transition density as

$$\gamma^{NM} = \begin{pmatrix} \mathbf{K}^{NM,\mathrm{occ}} & \mathbf{X}^{NM} \\ (\mathbf{Y}^{NM})^T & \mathbf{K}^{NM,\mathrm{virt}} \end{pmatrix}, \tag{37}$$

where $\mathbf{K}^{NM}$ is the block-diagonal unrelaxed transition density and $\mathbf{X}^{NM}$ and $\mathbf{Y}^{NM}$ describe orbital relaxations. Defining R^N and L^N in analogy to $R^{(\alpha)}$ and $L^{(\alpha)}$, and using the fact that changing the sign of the response frequency switches X and Y, the unrelaxed state-to-state transition density

matrix becomes

$$K_{ij}^{+NM} = -\frac{1}{4}\sum_{a}\Big[R_{ia}^{N}R_{ja}^{M} + L_{ia}^{N}L_{ja}^{M} + (N \leftrightarrow M)\Big], \tag{38a}$$

$$K_{ij}^{-NM} = \frac{1}{4}\sum_{a}\Big[L_{ia}^{M}R_{ja}^{N} + R_{ia}^{M}L_{ja}^{N} - (N \leftrightarrow M)\Big], \tag{38b}$$

$$K_{ab}^{+NM} = \frac{1}{4}\sum_{i}\Big[R_{ia}^{N}R_{ib}^{M} + L_{ia}^{N}L_{ib}^{M} + (N \leftrightarrow M)\Big], \tag{38c}$$

$$K_{ab}^{-NM} = \frac{1}{4}\sum_{a}\Big[L_{ia}^{M}R_{ib}^{N} + R_{ia}^{M}L_{ib}^{N} - (N \leftrightarrow M)\Big]. \tag{38d}$$

In contrast to the quadratic response function case, the skew-symmetric part of K^{NM} is antisymmetric with respect to exchange of N and M.

The orbital relaxation terms (off-diagonal blocks of the transition density) are the solution to the response equation

$$|X^{NM}, Y^{NM}\rangle = (\Lambda - \Omega_{MN}\Delta)^{-1}|P^{NM}, Q^{NM}\rangle, \tag{39}$$

where

$$\begin{aligned}(P+Q)_{ia}^{NM} = &-\frac{1}{2}\sum_{j}\left[R_{ja}^{M}H_{ji}^{+}[R^{N}] + L_{ja}^{M}H_{ji}^{-}[L^{N}] + (N \leftrightarrow M)\right] \\ &+\frac{1}{2}\sum_{b}\left[R_{ib}^{M}H_{ab}^{+}[R^{N}] + L_{ib}^{M}H_{ab}^{-}[L^{N}] + (N \leftrightarrow M)\right] \\ &+H_{ia}^{+}[K^{+NM}] + 2g_{ia}^{xc}[R^{N}, R^{M}],\end{aligned} \tag{40a}$$

$$\begin{aligned}(P-Q)_{ia}^{NM} = &\ \frac{1}{2}\sum_{j}\left[L_{ja}^{M}H_{ji}^{+}[R^{N}] + R_{ja}^{M}H_{ji}^{-}[L^{N}] - (N \leftrightarrow M)\right] \\ &-\frac{1}{2}\sum_{b}\left[L_{ib}^{M}H_{ab}^{+}[R^{N}] + R_{ib}^{M}H_{ab}^{-}[L^{N}] - (N \leftrightarrow M)\right] \\ &-H_{ia}^{-}[K^{-NM}],\end{aligned} \tag{40b}$$

and $\Omega_{MN} \equiv \Omega_M - \Omega_N$. Again, in contrast to $(P-Q)^{(\alpha\beta)}$, $(P-Q)^{NM}$ is anti-symmetric with respect to exchange of N and M. The previous equations generalize Eq. (57) in Ref. 3 and include a term

erroneously omitted in Ref. 3.

Applying the spectral representation of the linear response operator,

$$|X^{NM}, Y^{NM}\rangle = \sum_K \Big[|X^K, Y^K\rangle \frac{\langle X^K, Y^K | P^{NM}, Q^{NM}\rangle}{\Omega_{NM} - \Omega_K} + |Y^K, X^K\rangle \frac{\langle Y^K, X^K | P^{NM}, Q^{NM}\rangle}{\Omega_{NM} + \Omega_K} \Big] \tag{41}$$

one sees that the transition density matrix diverges when

$$|\Omega_{MN}| - \Omega_K \to 0. \tag{42}$$

Such behavior is unphysical since transition density matrices must always be finite.[27] Two routes to circumvent these unphysical divergences during simulations of excited state absorption spectra are explored in this work. In the first, the orbital relaxation is treated statically which is referred to as the pseudowavefunction (PW) approach.[38] This is similar to Li and Liu's equation-of-motion[39,40] formulation of state-to-state derivative couplings but differs from their state-to-state properties by including the orbital relaxation in the one-particle transition density matrix. Operationally, PW couplings are equivalent to setting Ω_{MN} to 0 in Eq. (39):

$$|X^{NM,\mathrm{pw}}, Y^{NM,\mathrm{pw}}\rangle = \Lambda^{-1} |P^{NM}, Q^{NM}\rangle. \tag{43}$$

Computing the transition density within response theory, $\boldsymbol{\rho}^{NM}$, and within PW, $\boldsymbol{\rho}^{NM,\mathrm{pw}}$, require the solution of the same number of linear response equations. However, when computing properties, significant computational savings can be realized by exploiting the fact that those linear response equations are at the same (zero) frequency. For example, the occupied-virtual contribution to the transition dipole moment can be rearranged by applying the inverse linear response operator to the left,

$$v_{NM}^{(\alpha),\mathrm{ov}} = \langle v^{(\alpha)} | X^{NM,\mathrm{pw}}, Y^{NM,\mathrm{pw}}\rangle = \langle X^{(\alpha)}, Y^{(\alpha)} | P^{NM}, Q^{NM}\rangle, \tag{44}$$

where the superscript "ov" indicates the occupied-virtual contribution and $X^{(\alpha)}$ and $Y^{(\alpha)}$ are static polarizability vectors, such that only one solution to a linear response equation is required *per property* rather than per pair of states.

Finally, we will also explore unrelaxed state-to-state transition properties, which are obtained by ignoring the orbital relaxation terms. Unrelaxed properties are inexpensive since they require no additional solution of a linear response equation, but are inconsistent with any derivative based properties and tend to overestimate transition properties, as is shown below.

2 Implementation

In this section, we outline the overall algorithm for all three second-order calculations and discuss several implementation details related to the use of symmetry in reducing the computational cost of hyperpolarizability and two-photon absorption calculations. The implementation detailed here builds on existing implementations of linear response properties and their gradients in Turbomole.[41] Calculations can be performed with spin-restricted or spin-unrestricted orbitals; with or without the resolution-of-the-identity approximation for Coulomb integrals[42,43] (RI-J); within full TDDFT or the Tamm–Dancoff approximation[44] (TDA); and for Hartree–Fock as well as DFT. Elements of the static hyperpolarizability were verified against finite-field derivatives of the total energy, dipole moment, and static polarizability. Hyperpolarizability tensors with a single zero-frequency were verified against finite-field derivatives of the dynamic polarizability through $\boldsymbol{\beta}(\omega, 0) = \frac{d}{dE}\boldsymbol{\alpha}(\omega)$. All second-order right-hand-sides (RHSs) as well as final amplitudes were additionally verified against sum-over-states representations obtained by inserting the spectral representation of the linear response operator and polarization vectors.

The most time-consuming steps of second-order response calculations are identical to operations that appear in linear response: solution of the symplectic eigenvalue equation, Eq. (20), or solution of a linear system of equations, Eqs. (14) and (39). Algorithms to iteratively diagonalize large matrices or solve large linear system of equations within TDDFT are well established; ours

is integral driven[45–49] and uses a nonorthonormal Krylov subspace method[50–52] such that the total cost scales asymptotically quadratically with system size, sublinearly with the number of solutions requested, and is comparable to the cost of ground state calculations. All RHS vectors are computed once and stored on disk. Molecular point-group symmetry is exploited in the molecular orbital basis by Clebsch-Gordan reduction of the molecular orbital products.[45] The symmetry-adapted $(A \pm B)_{ia,jb}$ matrix elements are nonzero only if the direct product of the irreps containing i and a contain the product of j and b. All matrix-vector products were performed in the atomic orbital basis, in which symmetry is exploited using skeleton operator techniques.[53,54] This leads to a speed up roughly the same order as that of the point-group. The next most time-consuming steps are the construction of the second-order RHSs, Eq. (28) and (40), which are evaluated as in Ref. 55.

2.1 Hyperpolarizability and two-photon absorption

Since the hyperpolarizability and two-photon absorption amplitudes share the same RHS, the general outline of both calculations differ primarily in the first step (where for 2PA, excited states must first be computed) and the last (where the inner product in 2PA is between the RHS and an excitation vector while for hyperpolarizability it is between the RHS and the polarization vector and the sum frequency). Thus, we discuss both algorithms simultaneously.

Consider first the full hyperpolarizability tensor, $\boldsymbol{\beta}(\omega_1, \omega_2)$, with a set of n_p unique perturbations, where

$$\beta_{\mu\nu\tau}(\omega_1, \omega_2) = \langle\langle v^{(\tau)}; v^{(\mu)}(\omega_1), v^{(\nu)}(\omega_2)\rangle\rangle. \tag{45}$$

In general, the hyperpolarizability tensor will have n_p^3 elements. However, since the quadratic response function is symmetric with respect to simultaneous permutations of perturbation operators and frequencies, e.g.,

$$\langle\langle v^{(\gamma)}; v^{(\alpha)}(\omega_\alpha), v^{(\beta)}(\omega_\beta)\rangle\rangle = \langle\langle v^{(\gamma)}; v^{(\beta)}(\omega_\beta), v^{(\alpha)}(\omega_\alpha)\rangle\rangle, \tag{46}$$

the number of unique elements is reduced if any of the frequencies are repeated. For example, the full dipole hyperpolarizability ($n_p = 3$) contains 27 elements, but only 10 of them are unique if both input frequencies are zero. Point-group symmetry further reduces the number of unique elements in the hyperpolarizability. Similarly, the two-photon absorption tensor $\mathbf{v}_{0K}(\omega)$ has, in the general case, n_p^2 unique elements which is reduced to $\frac{1}{2}n_p(n_p+1)$ when $\omega = \Omega_K/2$.

Both hyperpolarizability and 2PA require the computation of several polarization vectors. $n_X = n_p n_\omega$ distinct polarization vectors are required, where for the hyperpolarizability n_ω is the number of distinct frequencies in the set $\{\omega_1, \omega_2, \omega_1 + \omega_2\}$ and for 2PA, n_ω is the number of distinct frequencies in $\{\omega, \Omega_K - \omega\}$. In the hyperpolarizability case, ω_1 and ω_2 are specified freely by the user, while in the 2PA case, only ω is freely chosen.

With the polarization vectors determined, the RHS vectors, $P^{(\alpha\beta)}$ and $Q^{(\alpha\beta)}$, must be formed. To minimize the number of RHS vectors needed to compute the hyperpolarizability with a given frequency pair (ω_1, ω_2), the RHS is decomposed according to frequency and point-group symmetry. First, the n_p^2 RHS vectors are transformed so as to be explicitly symmetric ($S^{+\mu\nu}$) or antisymmetric ($S^{-\mu\nu}$) with respect to exchange of perturbation (but not frequency),

$$|S^{\pm\mu\nu}\rangle = \frac{1}{2}\left(|P^{(\mu\nu)}, Q^{(\mu\nu)}\rangle(\omega_1,\omega_2) \pm |P^{(\nu\mu)}, Q^{(\nu\mu)}\rangle(\omega_1,\omega_2)\right), \tag{47}$$

where $|P^{(\mu\nu)}, Q^{(\mu\nu)}\rangle(\omega_1,\omega_2)$ is the result of evaluating Eq. (28) with $(\nu^{(\alpha)}, \omega_\alpha) = (\nu^{(\mu)}, \omega_1)$ and $(\nu^{(\beta)}, \omega_\beta) = (\nu^{(\nu)}, \omega_2)$. $S^{-\mu\nu}$ is a Kleinman symmetry forbidden contribution to the hyperpolarizability and 2PA that vanishes when $\omega_1 = \omega_2$. Thus, when $\omega_1 = \omega_2$, the number of necessary RHS vectors is immediately reduced. The (anti)symmetrized RHS vectors are then conveniently decomposed into irreducible representations (irrep), where a further reduction in the number of RHS vectors can be accomplished by neglecting those RHS vectors that belong to an irrep orthogonal to the entire original set of perturbation operators (hyperpolarizability) or to the excited-state of interest (2PA).

The final hyperpolarizability or 2PA tensor is obtained by computing the inner products, and

transforming the full tensor from the irreducible basis to the Cartesian basis.

For example, consider the computation of the dipole hyperpolarizability. First, the $3n_\omega$ distinct first order polarization vectors must be computed. Next, the RHS vectors must be constructed. If $\omega_1 \neq \omega_2$, then both the symmetric and anti-symmetric RHS vectors must be constructed, whereas only the symmetric vectors are necessary if $\omega_1 = \omega_2$. In the case of the dipole hyperpolarizability, the 6 symmetric RHS vectors transform as the 6 unique elements of the polarizability tensor and the 3 antisymmetric RHS vectors transform as magnetic moments. Finally, the hyperpolarizability tensor constructed as in Eq. (33).

On the other hand, computation of the 2PA tensor starts with the calculation of all excited states of interest. Then 3 polarization vectors (x, y, and z) are computed for each unique ω and $\Omega_K - \omega$ for all states of interest, K. The RHS is constructed identically to the hyperpolarizability RHS, with $\omega_1 = \omega$ and $\omega_2 = \Omega_K - \omega$, and finally the 2PA amplitudes are constructed as in Eq. (35).

Table 1: Number of unique frequencies (n_ω), first-order polarizations (n_X), and right-hand sides (n_P) required to compute a general hyperpolarizability with p distinct perturbations and the dipole hyperpolarizability ($p = 3$) in accordance with the $2n+1$ rule, as well as the number of symmetry distinct elements for different choices of frequencies.

	$\omega_1 \neq \omega_2 \neq 0$	$\omega_1 = 0 \neq \omega_2$	$\omega_1 = \omega_2 \neq 0$	$\omega_1 = \omega_2 = 0$
n_ω	3	2	2	1
General hyperpolarizability				
n_X	$3p$	$2p$	$2p$	p
n_P	$3p$	$3p$	$2p$	$2p$
rank(β)	p^3	$\frac{1}{2}p^2(p+1)$	$\frac{1}{2}p^2(p+1)$	$\frac{(p+2)!}{3!(p-1)!}$
Dipole hyperpolarizability				
n_X	9	6	6	3
n_P	9	9	6	6
rank(β)	27	18	18	10

2.2 Excited-state absorption

Regardless of which formulation used, the first step of computing excited-state absorption amplitudes is to calculate all excited states of interest. The excitation vectors directly determine the

unrelaxed transition density, such that there is essentially no significant additional cost in computing the unrelaxed ESA amplitudes relative to the ground-state absorption amplitudes.

For the full response theory based ESA amplitudes as well as for the PW based amplitudes, two algorithms are possible. Both require the RHS shown in Eq. (40). In the first, the off-diagonal blocks of the transition density are determined by solving Eq. (39) for response amplitudes or Eq. (44) for PW amplitudes. In either case, the number of polarizability-like calculations required is n_{exc}, where n_{exc} is the number of excited-state amplitudes requested. This approach yields the full transition density matrix from which any transition properties are easily computed. The second approach avoids the formation of the transition density in favor of computing (dynamic) polarizability vectors for all properties of interest that are then contracted with the RHS. This approach requires the solution of $n_p n_\omega$ polarizability-like calculations where n_p is the number of one-electron properties desired and n_ω is the number of unique frequencies encountered. For response properties, n_ω is the number of unique energy differences among all requested amplitudes (generally $n_\omega = n_{\text{exc}}$), whereas for PW properties $n_\omega = 1$.

3 ESA: perylene diimide dimers

We now use our implementation to study the excited-state absorption spectra during excimer formation of a cofacially- and a slip-stacked perylene diimide (PDI) dimer on a triptycene scaffold shown in Fig. 1. Such chromophore dimers are valuable models to study charge- and energy-transfer in artificial light harvesting systems and materials for solar energy capture. The structures shown in Fig. 1 are derived from a pair of dimers first synthesized and studied spectroscopically by Margulies et al,[56] but in the present case the *n*-octyl groups bound to the imide nitrogen are replaced with methyl.

First, we compare the qualitative behaviors of the spectra provided by the quadratic response, pseudowavefunction, and unrelaxed formulations of state-to-state properties, all of which were computed with the implementation detailed above. Fig. 2 shows the excited-state absorption spec-

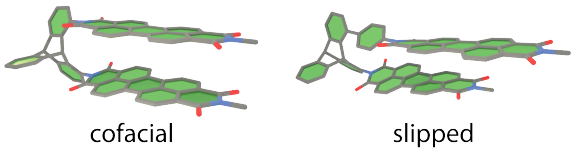

Figure 1: Structures of perylene diimide (PDI) structures for which excited state absorption spectra are computed.

tra computed using the PBE0 density functional[57] with the def2-SVP basis set[58] for both dimers in their ground state geometry. All excited-state absorption spectra in this section were broadened using a Lorentzian with full-width-at-half-maximum of 0.2 eV. Ground state geometries were obtained by optimizing with the TPSS density functional[59] including D3 dispersion corrections[60] and the def2-TZVP[58] basis set. As an example of the computational requirements, computing excited-state absorption amplitudes of the cofacial dimer from the first excited state to the next 10 singlet states (11 excited states, 10 amplitudes) with PBE0/def2-SVP and within response theory required 32 hours on a single core of an Intel Xeon X5660 with 2.80GHz clock speed. The most striking feature of Fig. 2 is the giant absorption peak at 599 nm in the excited-state absorption of the slip-stacked dimer computed from response theory, which has been scaled down by a factor of 2000 to facilitate comparison with the other spectra. The giant absorption is an unphysical artifact of the accidental matching condition Eq. (42): here, $|(\Omega_{69} - \Omega_1) - \Omega_1| < 0.25mH$. This spurious resonance is a severe failure made worse by its proximity to real transitions of interest and its presence at the ground state geometry. The PW-based spectra, on the other hand, are well behaved across the entire window. Furthermore, far from the matching condition of Eq. (42), the response and PW spectra are nearly identical while the unrelaxed spectra are consistently larger (up to a factor of 5), indicating that the orbital relaxation terms are comparable in magnitude to the unrelaxed terms and that the PW formulation captures a significant portion of the orbital relaxation.

Next, we consider the effect of structural relaxation on the excited-state absorption spectra by simulating excited-state absorption at the relaxed excited-state geometry. Both excited-state geometries were obtained by optimizing the first excited-state (S_1) geometry using PBE0-D3[57,60] with the def2-SVP[58] basis set. We focus on the PW spectra because it is well behaved and ap-

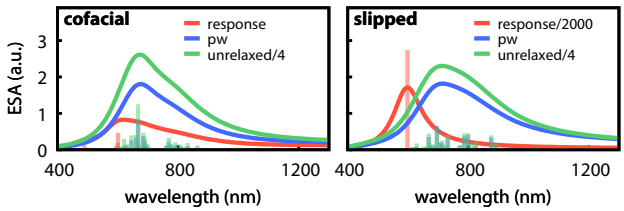

Figure 2: Comparison of excited-state absorption spectra computed using quadratic response ("response"), pseudowavefunction ("pw"), and unrelaxed state-to-state properties for the cofacial- and slip-stacked PDI dimers in their ground state geometries. All calculations used the PBE0 density functional[57] was used with the def2-SVP basis set.[58] Spectra were broadened with a Lorentzian with full-width-at-half-maximum of 0.2 eV. Note that response spectra for the slip-stacked dimer was scaled by 1/2000 and both unrelaxed spectra were scaled by 0.25.

proximately includes orbital relaxation. Fig. 3 compares the excited-state absorption spectra from the ground-state geometry and the excited-state geometry for both molecules. All excited-state absorption spectra were computed with PBE0[57] and def2-TZVPP.[58] With this basis set, the cofacial- and slipped-stacked dimers contain 3018 and 3260 basis functions, respectively.

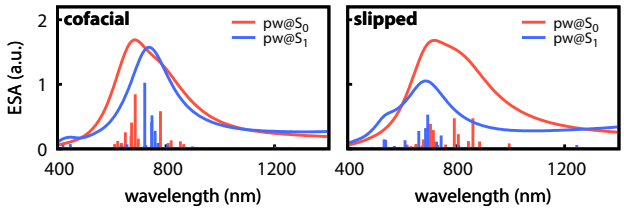

Figure 3: Simulated excited-state absorption during excimer formation in cofacial- and slipped-stacked PDI dimers at their ground state and relaxed excited-state geometries. Excited-state absorption spectra were computed using PBE0/def2-TZVPP with the PW formulation of the transition amplitudes. Spectra were broadened with a Lorentzian with full-width-at-half-maximum of 0.2 eV.

Ultrafast transient absorption measurements of the cofacial-stacked dimer reveal that the initially broad excited-state absorption centered at 667 nm sharpens and slightly blue shifts to 665 nm—a shift of 6 meV—as the excimer forms.[56] The simulated spectra recover the sharpening upon excimer formation as indicated by the reduction of the full-width-at-half-maximum (FWHM) from 0.66 eV at the ground state geometry to 0.47 eV at the excited state geometry. In contrast to the experimental behavior, the absorption maximum red shifts from 685 nm to 736 nm, a shift of 0.24 eV. This result is nonetheless encouraging, as both experiment and simulation agree that the shift

in the absorption maximum is slight. During excimer formation in the slip-stacked dimer, on the other hand, the initially sharp transient absorption peak centered at 707 nm becomes broad and relatively featureless,[56] while the simulated spectra is initially centered at 718 nm and slightly broadens upon excimer formation—FWHM of 0.72 eV at the ground state geometry compared to 0.76 eV at the excimer geometry.

4 2PA: twisted porphyrins

To demonstrate our two-photon absorption amplitude implementation, we compute the one-photon absorption (1PA) and two-photon absorption (2PA) spectra of a series of recently synthesized highly twisted π-conjugated porphyrins.[61] Specifically, we consider the porphyrin monomer (**mP**), dimer (**dP**), and tetramer (**tP**) with mesityl substitutions (i.e., compounds **1a**, **4a**, and **7** in Ref. 61), as shown in Fig. 4.

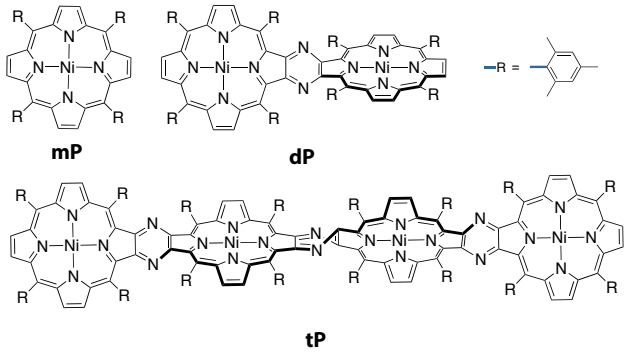

Figure 4: Structures of highly twisted porphyrin molecules. The monomer (**mP**), dimer (**dP**), and tetramer (**tP**) correspond to molecules **1a**, **4a**, and **7** in Ref. 61.

Previously reported crystal structures[61] were used as initial geometries for all compounds and were subsequently optimized using the TPSS density functional[59] with D3 dispersion corrections.[60] Final optimized structures were obtained with the def2-TZVP basis set[58] for **mP** and **dP**, while the def2-SVP basis set[58] was used for **tP** due to the large size of **tP**.

The one- and two-photon absorption spectra were computed using the hybrid PBE0 density functional[57] with def2-SVP,[58] except for **tP**, which used def2-SV(P). Computing two-photon ab-

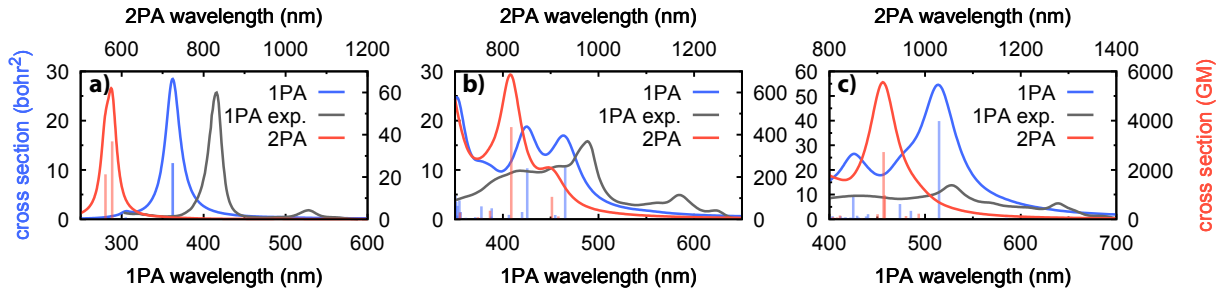

Figure 5: One-photon and two-photon absorption spectra of twisted porphyrins computed using TDDFT: a) **mP** b) **dP** c) **tP**. Simulated spectra were computed from response theory with PBE0[57] and def2-SVP (**mP** and **dP**) or def2-SV(P) (**tP**). Stick spectra were broadened with Lorentzian functions with half-width-at-half-maximum $\Gamma = 0.1$eV.

sorption amplitudes to the first 10 excited states of **mP** (equivalent of 10 excited state calculations followed by 10 dynamic polarizability calculations) required 44 hours on an Intel Xeon X5660 with 2.80GHz clock speed. Figure 5 collects one- and two-photon absorption spectra plotted as both stick spectra as well as broadened with a Lorentzian with half-width-at-half-maximum of 0.1 eV (see App. B). The stark differences between one- and two-photon absorption spectra are a consequence of the near inversion symmetry of the porphyrin rings. With perfect inversion symmetry, transitions can be one-photon active or two-photon active, but not both. Thus, in the case of the twisted porphyrins, transitions that are bright in the one-photon spectrum tend to be dark in the two-photon spectrum and vice versa. Both the experimentally obtained and TDDFT computed one-photon spectra show a pronounced red shift as the porphyrin chain elongates, corroborating the interpretation of the chain as being fully conjugated. In addition, TDDFT predicts an increasing maximum two-photon absorption cross section as the chain grows, in line with the expected increase of the absorption cross section with increasing conjugation length.[62] The computed maximum two-photon absorption cross section for **mP** (61 GM) is consistent with Yoon et al's observation that the two-photon absorption cross section of a similar Ni porphyrin was below 100 GM[63] and lies within the range of two-photon absorption cross sections measured for other porphyrin monomers (10 - 100 GM).[64] Furthermore, TDDFT predicts the two-photon absorption cross section of **dP** (the only molecule in the series in which two-photon absorption was measured) to be 690 GM which compares well with the experimentally observed value (640 GM at 1200 nm[61]).

The predicted maximum two-photon absorption of **tP**, 5600 GM, is larger by a factor of 7.8 than **dP**; in comparison, the observed absorption strength for a series of coplanar fused Ni porphyrin chains increased by a factor of 3.8 going between a dimer (8000 ± 200 GM) and a tetramer (29900 ± 600 GM).[63] Furthermore, the predicted two-photon absorption amplitudes for the twisted porphyrin chain are smaller by about an order of magnitude than those observed for the coplanar fused Ni porphyrin chains, which can be rationalized in terms of the significantly diminished degree of conjugation of the twisted porphyrin chain relative to the coplanar chain.[63]

The spurious pole in the quadratic response function manifests as an incorrect asymptotic resonance enhancement of the two-photon absorption spectra, i.e., the approximate two-photon absorption strengths are "over resonant". Consider the sum-over-states representation of the exact two-photon absorption amplitude,

$$v_{0N}^{(\alpha\beta)}(\omega)\Big|_{\omega=\Omega_N/2} = \sum_M \left[\frac{v_{0N}^{(\alpha)}\bar{v}_{NM}^{(\beta)} + v_{0N}^{(\beta)}\bar{v}_{NM}^{(\alpha)}}{\Omega_M - \Omega_N/2} \right], \tag{48}$$

with $\bar{v}_{NM}^{(\alpha)} = v_{NM}^{(\alpha)} - \delta_{NM} v_{00}^{(\alpha)}$. The two-photon absorption amplitude becomes strongly enhanced if there is an intermediate state, K, for which $\Omega_K \approx \Omega_N/2$. The corresponding transition strength grows asymptotically as

$$\delta_n^{2PA} \propto \frac{1}{\Delta\Omega^2} \tag{49}$$

for $\Delta\Omega = \Omega_K - \Omega_N/2$ (see App. A for a definition of δ_n^{2PA}). By contrast, analysis of Eq. (35) reveals that the TDDFT two-photon absorption transition strength is expected to grow asymptotically as

$$\delta_n^{2PA,\mathrm{TDDFT}} \propto \frac{1}{\Delta\Omega^4}. \tag{50}$$

To verify the incorrect asymptotic behavior numerically, we compute the near resonant transition strength of a modified **mP**. The resonance detuning, $\Delta\Omega$, was scanned by interpolating between the relaxed ground state geometry and the excited state geometry—optimized using PBE0[57] and def2-SVP.[58] To simplify the resulting spectra as well as reduce the computational cost of each

calculation, the mesityl groups were replaced with hydrogen atoms (after optimization), and both geometries were adapted to have D_{2d} symmetry. The interpolation between the ground state geometry and the excited state geometry was performed by linearly interpolating the symmetry unique internal coordinates. Fig. 6 shows δ_n^{2PA} for excitation to excited state $17A_1$ near a resonance with excited state $5E$, i.e., where $\Omega_{17A_1} \approx 2\Omega_{5E}$. Fitting the numerical transition strengths to the form $\log(\delta_n) = m \log|\Delta\Omega| + b$ yields $m = -4.0005$, or $\delta_n \propto \frac{1}{\Delta\Omega^{4.0005}}$. The fit was limited to points where δ_n was greater than 10^{11} a.u. (to focus on the single resonant contribution) but less than 10^{15} a.u. (to avoid numerical noise).

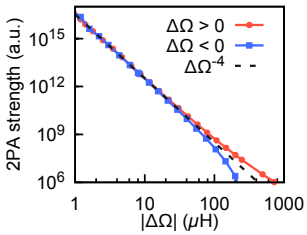

Figure 6: Resonant behavior of two-photon absorption strength computed through quadratic response TDDFT.

The overly resonant behavior seen above is analagous to the inconsistency in behavior of two-photon absorption cross sections near one-photon transitions reported by Hu et al within damped response theory.[18] Explicit damping, for example through the complex polarization propagator, is a commonly employed strategy to remove *physical* divergences in response functions by supposing a finite excited-state lifetime.[10,65] However, explicit damping does not change the underlying pole structure of the approximate response function, only how the pole structure translates into an observable, and therefore cannot cure *unphysical* behavior.

5 Hyperpolarizability: octupolar calixarenes

To demonstrate our implementation of the dynamic hyperpolarizability, we compute the hyperpolarizability at two frequencies for four conformational isomers of the cyclophane tetranitrotetrapropxycalix[4]arene shown in Fig. 7. These molecules have previously been experimentally

shown to have large second-order responses[66,67] and are therefore interesting prototypical nonlinear optically active chromophores.

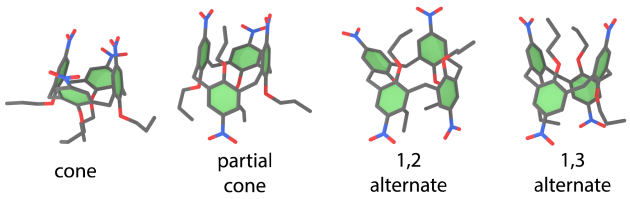

Figure 7: Octupolar calix[4]arene molecules for which hyperpolarizabilities are reported.

Molecular geometries were optimized using the TPSS density functional[59] with dispersion corrections[60] and the def2-TZVP basis set.[58] Hyperpolarizabilities were computed using the PBE0 density functional[57] with split valence[58] (def2-SVP, def2-TZVP) and diffuse property-optimized[68] (def2-SVPD, def2-TZVPD) basis sets. As an example of the efficiency of our implementation, computing the dynamic hyperpolarizability at two frequencies (1064 nm and 900 nm) for the cone isomer and def2-SVP basis required 12 hours on a single core of an Intel Xeon X5660 with 2.80GHz clock speed. To facilitate direct comparison with experimental Hyper-Raleigh scattering (HRS) results, we decompose the rank 3 hyperpolarizability tensor into rotational invariants before computing the HRS signal (see App. B). Assuming Kleinman symmetry (i.e., the hyperpolarizability is symmetric with respect to any permutation of indices), the hyperpolarizability can be exactly decomposed as a vector (dipolar) and a septor (octupolar) part,

$$\boldsymbol{\beta} = \boldsymbol{\beta}^{(1)} + \boldsymbol{\beta}^{(3)}, \tag{51}$$

and HRS is sensitive to both components.

Fig. 8 compares the computed results to the nanosecond HRS (nHRS) measurements with 1064nm light and femtosecond HRS (fHRS) measurements with 900nm light as well as simulated results using an additive model reported by Kenis et al.[67] Within the additive model, the hyperpolarizability for the complex is constructed as a sum of the individual p-propoxynitrobenzene moieties. Since the hyperpolarizabilities from the additive model were scaled such that the simu-

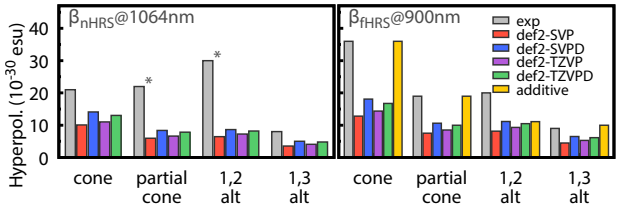

Figure 8: Hyperpolarizabilities computed with PBE0[57] functional and several basis sets compared to results from an additive model and Hyper-Raleigh scattering (HRS) experiments.[67] Experimental results at 1064nm (left) were obtained from nanosecond HRS while results at 900nm (right) were obtained from femtosecond HRS.[67] Nanosecond HRS measurements of the partial cone and 1,2 alt contain fluorescence contributions and therefore overestimate the pure hyperpolarizability contribution. Results from the additive model were uniformly scaled so that the simulated and experimental results for the cone agree.[67]

lated and experimental results for the cone conformation are identical, we consider only the trends given by the additive model. The computed signals at 1064nm for the cone and 1,3 alt conformers are consistent with the experimental nHRS results, while the computed and measured signals for the partial cone and 1,2 alt differ significantly. However, Kenis et al observed significant fluorescence in the nHRS experiments for the partial cone and 1,2 alt, suggesting that the reported hyperpolarizabilities for these two conformers overestimate the actual molecular hyperpolarizability. The fHRS measurements at 900nm, on the other hand, reduced the fluorescence contribution by integrating in a time-window (0.3 ns) much shorter than the fluorescence lifetime (2 ns).[67] We therefore focus our discussion on the fHRS results. On the positive side, the computed hyperpolarizabilities reproduce the experimental trend—cone > 1,2 alt > partial cone > 1,3 alt—for every basis set considered. In contrast, the additive model predicted the hyperpolarizability of 1,2 alt to be significantly lower than that of the partial cone. The discrepancy between the experimental results and the additive model was explained by a combination of conformational flexibility and an incomplete suppression of fluorescence; however, the present results suggest non-additive effects may be responsible.

Finally, two properties of basis set dependence of the hyperpolarizability are apparent from Fig. 8. First, the hyperpolarizability is strongly sensitive to diffuse functions in the basis set; for example, the computed HRS signals increased by 34–45% going from def2-SVP to def2-SVPD,

and by 13–18% going from def2-TZVP to def2-TZVPD. Second, unlike the polarizability,[69,70] the first hyperpolarizability obeys no variational principle. As a consequence, the hyperpolarizability does not converge monotonically towards the basis set limit. For example, in all computed results shown here, the hyperpolarizability computed with the largest basis set (def2-TZVPD) is intermediate between the values for two different proper subsets (def2-SVPD and def2-TZVP).

6 Conclusions

An efficient implementation of the quadratic response function, including the calculation of two-photon and excited-state absorption amplitudes, that makes full use of non-Abelian as well as Abelian point-group symmetries was detailed. Importantly, the schemes discussed here compute second-order response properties at a cost which is a fixed system-independent multiple of the corresponding first-order properties. The dipole hyperpolarizability requires at most three times the number of first-order polarization vector calculations as as a calculation of the dipole polarizability, all of which can be performed simultaneously owing to the $2n + 1$ rule.[71] Two-photon absorption amplitudes require at most the equivalent of two polarizability calculations per amplitude in addition to the initial excited state calculation. Excited-state absorption amplitudes require a single CPKS-like step per amplitude (in addition the initial excited state calculation) meaning an excited-state absorption spectrum from a given excited state is roughly twice the cost of the corresponding ground state spectrum. Furthermore, within the PW formulation, the excited-state absorption spectrum requires only the equivalent of an additional static polarizability calculation, hence providing the excited-state absorption spectrum for nearly the same cost as the ground-state absorption spectrum. Thus second-order properties are accessible for any systems for which first-order properties can be computed; the largest molecule considered here contained 446 atoms and 3932 basis functions (**tP**).

To demonstrate the reach of our implementation, we simulated excited-state absorption spectra during excimer formation in two perylene-diimide dimers, one- and two-photon absorption spectra

for a series of twisted porphyrins, and the dynamic hyperpolarizability of octupolar calix[4]arenes. The unphysical divergence in the excited-state absorption spectra was readily apparent in the excited-state absorption spectrum of the slip-stacked perylene diimide molecule, in which the spectrum was dominated by a single spurious peak that masked all other features even at the ground state geometry. On the other hand, the PW formulation yields well behaved spectra with no divergences and reproduces qualitative features of experimentally observed excimer formation.

The one- and two-photon absorption spectra of the twisted porphyrin series reproduce the qualitative features of the experimental spectra, including the increase of the two-photon absorption cross-section upon extending the monomer into a dimer.[61,63] In addition, the computed maximum two-photon absorption cross sections semiquantitatively reproduce the values observed experimentally.

The TDDFT simulated dipole hyperpolarizability agrees well with measured hyper-Raleigh scattering signals for the series of calix[4]arenes considered here. The simulated hyper-Raleigh scattering signal were within about a factor of two of the experimental results and in addition, the correct trend of cone > 1,2 alt > partial cone > 1,3 alt was recovered. In contrast, a previously reported additive model predicted a reversal of the partial cone and 1,2 alt, i.e., partial cone > 1,2 alt. Furthermore, our results exhibited a strong basis set dependence and non-monotonic convergence of the hyperpolarizability, indicating that diffuse functions are as vital to the reliable description of hyperpolarizabilities as they are to polarizabilities.

Our results provide further evidence that the incorrect pole structure of approximate nonlinear response functions is more than a fundamental curiosity but has serious and far-reaching consequences for the simulation of nonlinear properties in molecular systems. However, if the spurious poles are avoided, either through the PW formulation or fortuitously, the TDDFT results are semiquantitative, which is often sufficient for screening or modeling purposes. Our implementation will be available in a future release of TURBOMOLE, thus enabling nonlinear TDDFT-based properties for systems with hundreds of atoms and thousands of basis functions.

Acknowledgement

This material is based upon work supported by the U.S. Department of Energy, Office of Basic Energy Sciences, under Award Number DE-SC0018352. S.M.P. is supported by an Arnold O. Beckman Postdoctoral Fellowship.

A Two-photon absorption cross sections

The two-photon absorption cross section has dimensions of [length]^4[time] and is typically reported in Göppert-Mayer (GM) units which are defined as 1 GM = 10^{-50} cm^4 s. The cross section with appropriate units is[72]

$$\sigma_{\mathrm{2PA}}(\omega) = \frac{\mathcal{N}\pi^3\alpha a_0^5}{c}\left(\frac{\omega}{\mathrm{Hartree}}\right)^2 \times \tag{52}$$

$$\sum_n \left[\left(\frac{\delta_n^{\mathrm{2PA}}}{\mathrm{a.u.}}\right)(L(2\omega - \Omega_n;\Gamma)\cdot \mathrm{Hartree})\right], \tag{53}$$

where α is the fine structure constant, a_0 the Bohr radius, c the speed of light, ω the photon frequency, δ_{2PA} the two-photon transition strength, and $L(\omega;\Gamma)$ the normalized lineshape function.

The two-photon transition strength to state n, δ_n^{2PA}, is given by

$$\delta_n^{\mathrm{2PA}} = F\delta_n^F + G\delta_n^G + H\delta_n^H, \tag{54}$$

where the averaged quantities are defined by

$$\delta_n^F = \frac{1}{30}\sum_{\alpha\beta} v_{0n}^{(\alpha\alpha)}(\Omega_n/2)v_{0n}^{(\beta\beta)}(\Omega_n/2), \tag{55}$$

$$\delta_n^G = \frac{1}{30}\sum_{\alpha\beta} v_{0n}^{(\alpha\beta)}(\Omega_n/2)v_{0n}^{(\alpha\beta)}(\Omega_n/2), \tag{56}$$

$$\delta_n^H = \frac{1}{30}\sum_{\alpha\beta} v_{0n}^{(\alpha\beta)}(\Omega_n/2)v_{0n}^{(\beta\alpha)}(\Omega_n/2), \tag{57}$$

and the values of the coefficients $\mathcal{N}$, F, G, and H are determined by the type of experiment be-

ing simulated. All results reported in this paper simulate a single-beam experiment with linearly polarized lasers, i.e., $\mathcal{N} = 4$ and $F = G = H = 2$.[72]

The line shape function must be normalized, i.e., $\int_{-\infty}^{\infty} d\omega L(\omega;\Gamma) = 1$. All spectra reported here use a Lorentzian line shape,

$$L(\omega;\Gamma) = \frac{1}{\pi}\frac{\Gamma}{\omega^2 + \Gamma^2}, \tag{58}$$

with broadening factor $\Gamma = 0.1$ eV.

B Hyperpolarizability measurements

In this section, rotationally invariant representations of the rank-3 hyperpolarizability tensor are presented and used to express the simulated hyper Raleigh-scattering (HRS) signal. However, since the values of individual elements of the tensor depend on molecular orientation and experiments typically measure orientationally averaged responses, it is convenient to work directly with rotationally invariant quantities.[73]

A rank-3 Cartesian tensor, $\mathbf{T}$, can be decomposed into

$$\mathbf{T} = \mathbf{t}^{(0)} + \mathbf{t}^{(1)} + \mathbf{t}^{(2)} + \mathbf{t}^{(3)}, \tag{59}$$

where $\mathbf{t}^{(0)}$ is the scalar component, $\mathbf{t}^{(1)}$ the vector component (with 3 subcomponents), $\mathbf{t}^{(2)}$ the deviator component (with 2 subcomponents), and $\mathbf{t}^{(3)}$ the septor component. These components naturally define the following scalar invariants:

- magnitude of the scalar, $|A|$, with

$$A = \frac{1}{6}\sum_{\alpha\beta\gamma} e_{\alpha\beta\gamma} T_{\alpha\beta\gamma}, \tag{60}$$

- norms of the three vectors, $|\vec{\tau}^1|$, $|\vec{\tau}^2|$, $|\vec{\tau}^3|$, with

$$\tau^1_\alpha = \sum_\beta T_{\alpha\beta\beta} \tag{61}$$

$$\tau^2_\alpha = \sum_\beta T_{\beta\alpha\beta} \tag{62}$$

$$\tau^3_\alpha = \sum_\beta T_{\beta\beta\alpha} \tag{63}$$

- the eigenvalues of the two traceless symmetric deviator matrices,

$$D^1_{\alpha\beta} = -\frac{1}{2}\sum_{\gamma\kappa}\left(e_{\alpha\gamma\kappa}T_{\kappa\gamma\beta} + e_{\beta\gamma\kappa}T_{\gamma\kappa\alpha}\right) - 2A\delta_{\alpha\beta} \tag{64}$$

$$D^2_{\alpha\beta} = -\frac{1}{2}\sum_{\gamma\kappa}\left(T_{\alpha\gamma\kappa}e_{\kappa\gamma\beta} + T_{\beta\gamma\kappa}e_{\gamma\kappa\alpha}\right) - 2A\delta_{\alpha\beta} \tag{65}$$

- root-mean-square of elements of septor,

$$t^{(3)}_{\alpha\beta\gamma} = \bar{T}_{\alpha\beta\gamma} - \frac{1}{5}\left(\tau'_\alpha\delta_{\beta\gamma} + \tau'_\beta\delta_{\alpha\gamma} + \tau'_\gamma\delta_{\alpha\beta}\right), \tag{66}$$

  where

$$\bar{T}_{\alpha\beta\gamma} = \frac{1}{6}\left(T_{\alpha\beta\gamma} + T_{\beta\gamma\alpha} + T_{\gamma\alpha\beta} + T_{\alpha\gamma\beta} + T_{\gamma\beta\alpha} + T_{\beta\alpha\gamma}\right), \tag{67}$$

  and

$$\vec{\tau}' = \frac{1}{3}\left(\vec{\tau}^1 + \vec{\tau}^2 + \vec{\tau}^3\right) \tag{68}$$

In the previous equations, **e**, is an antisymmetric tensor defined by

$$e_{\alpha\beta\gamma} = \begin{cases} 1 & \text{if } \alpha\beta\gamma \text{ an even permutation of } xyz \\ -1 & \text{if } \alpha\beta\gamma \text{ an odd permutation of } xyz \\ 0 & \text{otherwise} \end{cases} \tag{69}$$

Hyper-Raleigh scattering measures the intensity of scattered frequency-doubled light upon il-

lumination of an isotropic solution as a function of solute concentration.[74,75] The intensity of the scattered field is proportional to the sum of solvent and solute contributions as well as the square of the incident intensity,

$$I(2\omega) \propto \left(N_{\text{solvent}} \langle \beta^2_{\text{HRS}} \rangle_{\text{solvent}} + N_{\text{solute}} \langle \beta^2_{\text{HRS}} \rangle_{\text{solute}}\right) I(\omega)^2, \tag{70}$$

where N_{solvent} (N_{solute}) is the number density of the solvent (solute), $\langle \beta^2_{\text{HRS}} \rangle_{\text{solvent}}$ ($\langle \beta^2_{\text{HRS}} \rangle_{\text{solute}}$) is the squared orientationally averaged molecular hyperpolarizability signal of the solvent (solute), and $I(\omega)$ is the field intensity with frequency ω.[74]

Assuming Kleinman symmetry (i.e. the hyperpolarizability is symmetric with respect to exchange of any indices), the signal is sensitive to an isotropic average of the hyperpolarizability,[76]

$$\begin{aligned}
\langle \beta^2_{\text{HRS}} \rangle =& \frac{6}{35} \sum_{\alpha} \beta^2_{\alpha\alpha\alpha} + \frac{16}{105} \sum_{\alpha\neq\beta} \beta_{\alpha\alpha\alpha}\beta_{\alpha\beta\beta} \\
&+ \frac{38}{105} \sum_{\alpha\neq\beta} \beta^2_{\alpha\beta\beta} + \frac{16}{105} \mathcal{P}_{\text{cyc}} \beta_{\alpha\alpha\beta}\beta_{\beta\gamma\gamma} \\
&+ \frac{20}{35} \beta_{xyz} \qquad (71) \\
=& \frac{2}{15}|\tau'|^2 + \frac{2}{21}|\mathbf{t}^{(3)}|^2, \qquad (72)
\end{aligned}$$

where the last line is an equivalent expression in terms of the tensor invariants τ' and $\mathbf{t}^{(3)}$.

References

(1) Mukamel, S. *Principles of nonlinear optical spectroscopy*; Oxford University Press on Demand, 1999.

(2) Olsen, J.; Jørgensen, P. Linear and nonlinear response functions for an exact state and for an MCSCF state. *J. Chem. Phys.* **1985**, *82*, 3235.

(3) Furche, F. On the density matrix based approach to time-dependent density functional response theory. *J. Chem. Phys.* **2001**, *114*, 5982–5992.

(4) van Gisbergen, S. J. A.; Snijders, J. G.; Baerends, E. J. Time-dependent Density Functional Results for the Dynamic Hyperpolarizability of C_{60}. *Phys. Rev. Lett.* **1997**, *78*, 3097–3100.

(5) van Gisbergen, S. J. A.; Snijders, J. G.; Baerends, E. J. Calculating frequency-dependent hyperpolarizabilities using time-dependent density functional theory. *J. Chem. Phys.* **1998**, *109*, 10644–10656.

(6) van Gisbergen, S. J. A.; Fonseca Guerra, C.; Baerends, E. J. Towards excitation energies and (hyper)polarizability calculations of large molecules. Application of parallelization and linear scaling techniques to time-dependent density functional response theory. *J. Comput. Chem.* **2000**, *21*, 1511–1523.

(7) Sałek, P.; Vahtras, O.; Helgaker, T.; Ågren, H. Density-functional theory of linear and nonlinear time-dependent molecular properties. *J. Chem. Phys.* **2002**, *117*, 9630–9645.

(8) Hait Heinze, H.; Della Sala, F.; Görling, A. Efficient methods to calculate dynamic hyperpolarizability tensors by time-dependent density-functional theory. *J. Chem. Phys.* **2002**, *116*, 9624–9640.

(9) Tretiak, S.; Chernyak, V. Resonant nonlinear polarizabilities in the time-dependent density functional theory. *J. Chem. Phys.* **2003**, *119*, 8809–8823.

(10) Norman, P.; Bishop, D. M.; Jensen, H. J. A.; Oddershede, J. Nonlinear response theory with relaxation: the first-order hyperpolarizability. *J. Chem. Phys.* **2005**, *123*, 194103.

(11) Kussmann, J.; Ochsenfeld, C. A density matrix-based method for the linear-scaling calculation of dynamic second- and third-order properties at the Hartree-Fock and Kohn-Sham density functional theory levels. *J. Chem. Phys.* **2007**, *127*, 204103.

(12) Henriksson, J.; Saue, T.; Norman, P. Quadratic response functions in the relativistic four-component Kohn-Sham approximation. *J. Chem. Phys.* **2008**, *128*, 024105.

(13) Kjærgaard, T.; Jørgensen, P.; Olsen, J.; Coriani, S.; Helgaker, T. Hartree-Fock and Kohn-Sham time-dependent response theory in a second-quantization atomic-orbital formalism suitable for linear scaling. *J. Chem. Phys.* **2008**, *129*, 054106.

(14) Bast, R.; Saue, T.; Henriksson, J.; Norman, P. Role of noncollinear magnetization for the first-order electric-dipole hyperpolarizability at the four-component Kohn–Sham density functional theory level. *J. Chem. Phys.* **2009**, *130*, 024109.

(15) Hu, Z.; Autschbach, J.; Jensen, L. Simulation of resonance hyper-Rayleigh scattering of molecules and metal clusters using a time-dependent density functional theory approach. *J. Chem. Phys.* **2014**, *141*, 124305.

(16) Sałek, P.; Vahtras, O.; Guo, J.; Luo, Y.; Helgaker, T.; Ågren, H. Calculations of two-photon absorption cross sections by means of density-functional theory. *Chem. Phys. Lett.* **2003**, *374*, 446–452.

(17) Frediani, L.; Rinkevicius, Z.; Ågren, H. Two-photon absorption in solution by means of time-dependent density-functional theory and the polarizable continuum model. *J. Chem. Phys.* **2005**, *122*, 244104.

(18) Hu, Z.; Autschbach, J.; Jensen, L. Simulating Third-Order Nonlinear Optical Properties Using Damped Cubic Response Theory within Time-Dependent Density Functional Theory. *J. Chem. Theory Comput.* **2016**, *12*, 1294–1304.

(19) Friese, D. H.; Beerepoot, M. T. P.; Ringholm, M.; Ruud, K. Open-Ended Recursive Approach for the Calculation of Multiphoton Absorption Matrix Elements. *J. Chem. Theory Comput.* **2015**, *11*, 1129–1144.

(20) Fahleson, T.; Ågren, H.; Norman, P. A Polarization Propagator for Nonlinear X-ray Spectroscopies. *J. Phys. Chem. Lett.* **2016**, 1991–1995.

(21) Cronstrand, P.; Christiansen, O.; Norman, P.; Ågren, H. Theoretical calculations of excited state absorption. *Phys. Chem. Chem. Phys.* **2000**, *2*, 5357–5363.

(22) Fischer, S. A.; Cramer, C. J.; Govind, N. Excited State Absorption from Real-Time Time-Dependent Density Functional Theory. *J. Chem. Theory Comput.* **2015**, *11*, 4294–4303.

(23) Falklöf, O.; Durbeej, B.; Norman, P. Inter-Excited-State Phosphorescence in the Four-Component Relativistic Kohn–Sham Approximation: A Case Study on Lumiflavin. *J. Phys. Chem. A* **2015**, *119*, 11911–11921.

(24) Oliveira, E. F.; Shi, J.; Lavarda, F. C.; Lüer, L.; Milián-Medina, B.; Gierschner, J. Excited state absorption spectra of dissolved and aggregated distyrylbenzene: A TD-DFT state and vibronic analysis. *J. Chem. Phys.* **2017**, *147*, 034903.

(25) Aidas, K.; Angeli, C.; Bak, K. L.; Bakken, V.; Bast, R.; Boman, L.; Christiansen, O.; Cimiraglia, R.; Coriani, S.; Dahle, P.; Dalskov, E. K.; Ekström, U.; Enevoldsen, T.; Eriksen, J. J.; Ettenhuber, P.; Fernández, B.; Ferrighi, L.; Fliegl, H.; Frediani, L.; Hald, K.; Halkier, A.; Hättig, C.; Heiberg, H.; Helgaker, T.; Hennum, A. C.; Hettema, H.; Hjertenæs, E.; Høst, S.; Høyvik, I.-M.; Iozzi, M. F.; Jansík, B.; Jensen, H. J. Aa.; Jonsson, D.; Jørgensen, P.; Kauczor, J.; Kirpekar, S.; Kjærgaard, T.; Klopper, W.; Knecht, S.; Kobayashi, R.; Koch, H.; Kongsted, J.; Krapp, A.; Kristensen, K.; Ligabue, A.; Lutnæs, O. B.; Melo, J. I.; Mikkelsen, K. V.; Myhre, R. H.; Neiss, C.; Nielsen, C. B.; Norman, P.; Olsen, J.; Olsen, J. M. H.; Osted, A.; Packer, M. J.; Pawlowski, F.; Pedersen, T. B.; Provasi, P. F.; Reine, S.; Rinkevicius, Z.; Ruden, T. A.; Ruud, K.; Rybkin, V. V.; Sałek, P.; Samson, C. C. M.; de Merás, A. S.; Saue, T.; Sauer, S. P. A.; Schimmelpfennig, B.; Sneskov, K.; Steindal, A. H.; Sylvester-Hvid, K. O.; Taylor, P. R.; Teale, A. M.; Tellgren, E. I.; Tew, D. P.; Thorvaldsen, A. J.; Thøgersen, L.; Vahtras, O.; Watson, M. A.; Wilson, D. J. D.; Ziolkowski, M.; Ågren, H. The Dalton quantum chemistry program system. *WIREs Comput. Mol. Sci.* **2014**, *4*, 269–284.

(26) Champagne, B.; Perpète, E. A.; Jacquemin, D.; van Gisbergen, S. J. A.; Baerends, E. J.;

Soubra-Ghaoui, C.; Robins, K. A.; Kirtman, B. Assessment of Conventional Density Functional Schemes for Computing the Dipole Moment and (Hyper)polarizabilities of Push-Pull π-Conjugated Systems . *J. Phys. Chem. A* **2000**, *104*, 4755–4763.

(27) Parker, S. M.; Roy, S.; Furche, F. Unphysical divergences in response theory. *J. Chem. Phys.* **2016**, *145*, 134105.

(28) Petersilka, M.; Gossmann, U. J.; Gross, E. K. U. Excitation Energies from Time-Dependent Density-Functional Theory. *Phys. Rev. Lett.* **1996**, *76*, 1212–1215.

(29) Gross, E. K. U.; Dobson, J. F.; Petersilka, M. *Density Functional Theory II*; Springer-Verlag: Berlin/Heidelberg, 1996; pp 81–172.

(30) Zangwill, A.; Soven, P. Density-functional approach to local-field effects in finite systems: Photoabsorption in the rare gases. *Phys. Rev. A* **1980**, *21*, 1561–1572.

(31) Casida, M. E. In *Recent advances in density functional methods*; Chong, D. P., Ed.; Recent advances in computational chemistry; World Scientific: Singapore, 1995; Vol. 1; Chapter Time-Dependent Density Functional Response Theory for Molecules, pp 155–192.

(32) Thorvaldsen, A. J.; Ruud, K.; Kristensen, K.; Jørgensen, P.; Coriani, S. A density matrix-based quasienergy formulation of the Kohn–Sham density functional response theory using perturbation- and time-dependent basis sets. *J. Chem. Phys.* **2008**, *129*, 214108.

(33) Runge, E.; Gross, E. K. U. Density-Functional Theory for Time-Dependent Systems. *Phys. Rev. Lett.* **1984**, *52*, 997–1000.

(34) Aiga, F.; Tada, T.; Yoshimura, R. Frequency-dependent polarizabilities, hyperpolarizabilities, and excitation energies from time-dependent density-functional theory based on the quasienergy derivative method. *J. Chem. Phys.* **1999**, *111*, 2878–2888.

(35) Furche, F.; Ahlrichs, R. Adiabatic time-dependent density functional methods for excited state properties. *J. Chem. Phys.* **2002**, *117*, 7433.

(36) Christiansen, O.; Jørgensen, P.; Hättig, C. Response functions from Fourier component variational perturbation theory applied to a time-averaged quasienergy. *Int. J. Quant. Chem.* **1998**, *68*, 1–52.

(37) Hättig, C.; Christiansen, O.; Jorgensen, P. Multiphoton transition moments and absorption cross sections in coupled cluster response theory employing variational transition moment functionals. *J. Chem. Phys.* **1998**, *108*, 8331.

(38) Ou, Q.; Alguire, E. C.; Subotnik, J. E. Derivative Couplings between Time-Dependent Density Functional Theory Excited States in the Random-Phase Approximation Based on Pseudo-Wavefunctions: Behavior around Conical Intersections. *J. Phys. Chem. B* **2015**, *119*, 7150–7161.

(39) Li, Z.; Liu, W. First-order nonadiabatic coupling matrix elements between excited states: a Lagrangian formulation at the CIS, RPA, TD-HF, and TD-DFT levels. *J. Chem. Phys.* **2014**, *141*, 014110.

(40) Li, Z.; Suo, B.; Liu, W. First order nonadiabatic coupling matrix elements between excited states: Implementation and application at the TD-DFT and pp-TDA levels. *J. Chem. Phys.* **2014**, *141*, 244105.

(41) TURBOMOLE V7.0 2015, a development of University of Karlsruhe and Forschungszentrum Karlsruhe GmbH, 1989-2007, TURBOMOLE GmbH, since 2007; available from `http://www.turbomole.com`.

(42) Baerends, E. J.; Ellis, D. E.; Ros, P. Self-consistent molecular Hartree—Fock—Slater calculations I. The computational procedure. *Chem. Phys.* **1973**, *2*, 41–51.

(43) Dunlap, B. I.; Connolly, J. W. D.; Sabin, J. R. On some approximations in applications of Xα theory. *J. Chem. Phys.* **1979**, *71*, 3396–3402.

(44) Hirata, S.; Head-Gordon, M. Time-dependent density functional theory within the Tamm–Dancoff approximation. *Chem. Phys. Lett.* **1999**, *314*, 291–299.

(45) Weiss, H.; Ahlrichs, R.; Häser, M. A direct algorithm for self-consistent-field linear response theory and application to C_{60}: Excitation energies, oscillator strengths, and frequency-dependent polarizabilities. *J. Chem. Phys.* **1993**, *99*, 1262–1270.

(46) Treutler, O.; Ahlrichs, R. Efficient molecular numerical integration schemes. *J. Chem. Phys.* **1995**, *102*, 346–354.

(47) Stratmann, R. E.; Scuseria, G. E.; Frisch, M. J. Achieving linear scaling in exchange-correlation density functional quadratures. *Chem. Phys. Lett.* **1996**, *257*, 213–223.

(48) van Gisbergen, S. J. A.; Snijders, J. G.; Baerends, E. J. Implementation of time-dependent density functional response equations. *Comput. Phys. Commun.* **1999**, *118*, 119–138.

(49) Görling, A.; Heinze, H. H.; Ruzankin, S. P.; Staufer, M.; Rösch, N. Density- and density-matrix-based coupled Kohn–Sham methods for dynamic polarizabilities and excitation energies of molecules. *J. Chem. Phys.* **1999**, *110*, 2785–2799.

(50) Stratmann, R. E.; Scuseria, G. E.; Frisch, M. J. An efficient implementation of time-dependent density-functional theory for the calculation of excitation energies of large molecules. *J. Chem. Phys.* **1998**, *109*, 8218–8224.

(51) Furche, F.; Ahlrichs, R.; Wachsmann, C.; Weber, E.; Sobanski, A.; Vögtle, F.; Grimme, S. Circular Dichroism of Helicenes Investigated by Time-Dependent Density Functional Theory. *J. Am. Chem. Soc.* **2000**, *122*, 1717–1724.

(52) Furche, F.; Krull, B. T.; Nguyen, B. D.; Kwon, J. Accelerating molecular property calculations with nonorthonormal Krylov space methods. *J. Chem. Phys.* **2016**, *144*, 174105.

(53) Dupuis, M.; King, H. F. Molecular symmetry and closed-shell SCF calculations. I. *Int. J. Quantum Chem.* **1977**, *11*, 613–625.

(54) Taylor, P. R. Symmetrization of operator matrix elements. *Int. J. Quantum Chem.* **1985**, *27*, 89–96.

(55) Rappoport, D.; Furche, F. Lagrangian approach to molecular vibrational Raman intensities using time-dependent hybrid density functional theory. *J. Chem. Phys.* **2007**, *126*, 201104.

(56) Margulies, E. A.; Shoer, L. E.; Eaton, S. W.; Wasielewski, M. R. Excimer formation in co-facial and slip-stacked perylene-3,4:9,10-bis(dicarboximide) dimers on a redox-inactive triptycene scaffold . *Phys. Chem. Chem. Phys.* **2014**, *16*, 23735–23742.

(57) Perdew, J. P.; Ernzerhof, M.; Burke, K. Rationale for Mixing Exact Exchange with Density Functional Approximations. *J. Chem. Phys.* **1996**, *105*, 9982.

(58) Weigend, F.; Ahlrichs, R. Balanced basis sets of split valence, triple zeta valence and quadruple zeta valence quality for H to Rn: Design and assessment of accuracy. *Phys. Chem. Chem. Phys.* **2005**, *7*, 3297.

(59) Tao, J.; Perdew, J.; Staroverov, V.; Scuseria, G. Climbing the Density Functional Ladder: Nonempirical Meta-Generalized Gradient Approximation Designed for Molecules and Solids. *Phys. Rev. Lett.* **2003**, *91*, 146401.

(60) Grimme, S.; Antony, J.; Ehrlich, S.; Krieg, H. A Consistent and Accurate Ab Initio Parametrization of Density Functional Dispersion Correction (DFT-D) for the 94 Elements H-Pu. *J. Chem. Phys.* **2010**, *132*, 154104.

(61) Ito, S.; Hiroto, S.; Lee, S.; Son, M.; Hisaki, I.; Yoshida, T.; Kim, D.; Kobayashi, N.; Shinokubo, H. Synthesis of Highly Twisted and Fully π-Conjugated Porphyrinic Oligomers. *J. Am. Chem. Soc.* **2015**, *137*, 142–145.

(62) Drobizhev, M.; Stepanenko, Y.; Rebane, A.; Wilson, C. J.; Screen, T. E. O.; Anderson, H. L. Strong Cooperative Enhancement of Two-Photon Absorption in Double-Strand Conjugated Porphyrin Ladder Arrays. *J. Am. Chem. Soc.* **2006**, *128*, 12432–12433.

(63) Yoon, M.-C.; Noh, S. B.; Tsuda, A.; Nakamura, Y.; Osuka, A.; Kim, D. Photophysics of meso-β Doubly Linked Ni(II) Porphyrin Arrays: Large Two-Photon Absorption Cross-Section and Fast Energy Relaxation Dynamics. *J. Am. Chem. Soc.* **2007**, *129*, 10080–10081.

(64) Pawlicki, M.; Collins, H. A.; Denning, R. G.; Anderson, H. L. Two-Photon Absorption and the Design of Two-Photon Dyes. *Angew. Chem. Int. Ed.* **2009**, *48*, 3244–3266.

(65) Norman, P.; Bishop, D. M.; Jorgen Aa Jensen, H.; Oddershede, J. Near-resonant absorption in the time-dependent self-consistent field and multiconfigurational self-consistent field approximations. *J. Chem. Phys.* **2001**, *115*, 10323.

(66) Kelderman, E.; Verboom, W.; Engbersen, J. F. J.; Reinhoudt, D. N.; Heesink, G. J. T.; van Hulst, N. F.; Derhaeg, L.; Persoons, A. Nitrocalix[4]arenes as Molecules for Second-Order Nonlinear Optics. *Angew. Chem. Int. Ed.* **1992**, *31*, 1075–1077.

(67) Kenis, P. J. A.; Noordman, O. F. J.; Houbrechts, S.; van Hummel, G. J.; Harkema, S.; van Veggel, F. C. J. M.; Clays, K.; Engbersen, J. F. J.; Persoons, A.; van Hulst, N. F.; Reinhoudt, D. N. Second-Order Nonlinear Optical Properties of the Four Tetranitrotetrapropoxycalix[4]arene Conformers. *J. Am. Chem. Soc.* **1998**, *120*, 7875–7883.

(68) Rappoport, D.; Furche, F. Property-optimized gaussian basis sets for molecular response calculations. *J. Chem. Phys.* **2010**, *133*, 134105.

(69) Hirschfelder, J. O.; Brown, W. B.; Epstein, S. T. Recent Developments in Perturbation Theory. *Adv. Quantum Chem.* **1964**, *1*, 255–374.

(70) Werner, H.-J.; Meyer, W. PNO-CI and PNO-CEPA studies of electron correlation effects. *Mol. Phys.* **1976**, *31*, 855–872.

(71) Wigner, E. On a modification of the Rayleigh–Schrödinger perturbation theory. *Math. Naturwiss. Anz. Ungar. Akad. Wiss.* **1935**, *35*, 477–482.

(72) Beerepoot, M. T. P.; Friese, D. H.; List, N. H.; Kongsted, J.; Ruud, K. Benchmarking two-photon absorption cross sections: performance of CC2 and CAM-B3LYP. *Phys. Chem. Chem. Phys.* **2015**, *17*, 19306–19314.

(73) Jerphagnon, J. Invariants of the Third-Rank Cartesian Tensor: Optical Nonlinear Susceptibilities. *Phys. Rev. B* **1970**, *2*, 1091–1098.

(74) Clays, K.; Persoons, A. Hyper-Rayleigh scattering in solution. *Phys. Rev. Lett.* **1991**, *66*, 2980–2983.

(75) Clays, K.; Persoons, A. Hyper-Rayleigh scattering in solution. *Rev. Sci. Instrum.* **1992**, *63*, 3285–3289.

(76) Bersohn, R.; Pao, Y. H.; Frisch, H. L. Double-Quantum Light Scattering by Molecules. *J. Chem. Phys.* **1966**, *45*, 3184–3198.

Graphical TOC Entry